MAD/PH/862
January 1995

NEUTRINOS FROM PRIMORDIAL BLACK HOLES

Francis Halzen and Bettina Keszthelyi
Physics Department, University of Wisconsin, Madison, WI 53706

Enrique Zas
Departamento de Física de Partículas, Universidad de Santiago
E-15706 Santiago de Compostela, Spain

Abstract

The emission of particles from black holes created in the early Universe has detectable astrophysical consequences. The most stringent bound on their abundance has been obtained from the absence of a detectable diffuse flux of 100 MeV photons. Further scrutiny of these bounds is of interest as they, for instance, rule out primordial black holes as a dark matter candidate. We here point out that these bounds can, in principle, be improved by studying the diffuse cosmic neutrino flux. Measurements of near-vertical atmospheric neutrino fluxes in a region of low geomagnetic latitude can provide a competitive bound. The most favorable energy to detect a possible diffuse flux of primordial black hole origin is found to be a few MeV. We also show that measurements of the diffuse ν_τ flux is the most promising to improve the existing bounds deduced from gamma-ray measurements. Neutrinos from individual black hole explosions can be detected in the GeV-TeV energy region. We find that the kilometer-scale detectors, recently proposed, are able to establish competitive bounds.

1 Introduction

Soon after Hawking described the quantum evaporation of black holes [1], it was suggested that emission from black holes, created in the early Universe, has detectable astrophysical consequences [2, 3, 4]. Such black holes are referred to as primordial. They may be formed by the collapse of density fluctuations at an early epoch [5], at a cosmic phase transition [6] or by more exotic mechanisms such as the collapse of closed cosmic strings [7]. Attempts were made to search the Hawking radiation from primordial black holes (PBHs). The instantaneous emission spectra [1] of particles by an individual black hole resemble a black body spectrum with temperature inversely proportional to the black hole mass. Only holes of masses below the critical mass $M_* \simeq 4 - 6 \times 10^{14}$ g evaporate within the age of the Universe through this mechanism.

In this paper we assume that a particle species is emitted when the black hole temperature exceeds the relevant rest mass and if the particle appears elementary at this temperature. A solar mass black hole emits only massless particles, photons and possibly neutrinos. As a black hole evaporates its temperature rises crossing the emission threshold of heavier particles so that new degrees of freedom are added to the emission. A black hole of mass M_* also emits electrons and positrons with energies in the $50 - 100$ MeV energy range. This average energy is sufficiently close to the muon and pion rest mass so that they are also kinematically accessible. In the Standard Model this means that the quark and gluon degrees of freedom will contribute to the radiation. When the temperature approaches Λ_{QCD} quarks and gluons are emitted freely which subsequently fragment into hadrons by mechanisms familiar from accelerator studies. Fragmentation products decay into stable particles which add to the direct Hawking emission, thus contributing an enhancement in the spectrum near $\simeq 140$ MeV, the pion rest mass [8].

PBHs can be searched for as nearby point sources or, alternatively, one may search for the accumulated diffuse flux of all PBHs which evaporated within the lifetime of our Universe. Page and Hawking obtained the first such bound from the requirement that this diffuse flux cannot exceed the observed gamma ray spectrum [2]. The most stringent bound is obtained for photons with energy of order 100 MeV. They only considered the direct photon flux. This result was later updated to include all Standard Model degrees of freedom as well as the fragmentation of quarks and gluons [8, 9].

Bounds obtained from the observed diffuse electron, positron and antiproton spectrum [4] are remarkably close to those from gamma rays.

Searches for individual, nearby holes provide bounds on explosion rates which are complementary to the diffuse bounds. These bounds depend on the possible clustering of PBHs around galaxies and on their final stage evolution which is dictated by yet unsettled high energy physics. Though the solutions to these problems are somewhat ambiguous, an observation of such an explosion would reveal all the degrees of freedom of all particles in the Universe irrespective of their mass.

The extension of the work on photons to include neutrinos is most natural. The construction of a new generation of solar and supernova neutrino detectors as well as the commissioning of a new type of high energy neutrino telescope provide us with novel ways to search for PBHs. The low cross sections for neutrino interactions require large detector volumes, but they also allow detection on the Earth's surface avoiding shielding by either the interstellar medium, the atmosphere or the Earth itself. The emission of direct neutrinos has been previously addressed by Carr [4]. In this work we include the production of neutrinos via the decay of hadrons. By comparing the diffuse neutrino fluxes from PBHs to the observed neutrino backgrounds we determine the most favorable energy regions for obtaining new independent bounds on PBH abundances. We will show that such regions of opportunity exist in the range of sensitivity of both low- and high energy neutrino telescopes.

2 Hawking radiation from PBHs and emission models

Hawking showed that a black hole emits particles thermally with a temperature that depends only on its mass, charge and angular momentum. We can safely assume that PBHs, formed in the early Universe, are neutral and nonrotating because any nonvanishing initial charge or angular momentum would have been lost soon after their formation. A black hole emits particles with energy in the range $(E, E + dE)$ at a rate [1]

$$\frac{\mathrm{d}^2 N}{\mathrm{d}t\mathrm{d}E} = \frac{1}{2\pi\hbar} \frac{\Gamma_s(E, M)}{\exp\left(8\pi GME/\hbar c^3\right) - (-1)^{2s}} \tag{1}$$

per particle degree of freedom. Here M is the mass of the hole, s is the particle spin and $\Gamma_s(E, M)$ is the absorption coefficient.

Although Eq. (1) does not represent a perfect black body spectrum because $\Gamma_s(E, M)$ is energy dependent, one can define a temperature

$$kT = \frac{\hbar c^3}{8\pi GM}. \tag{2}$$

The absorption coefficient $\Gamma_s(E, M)$ depends on E, M and s and any other internal degrees of freedom as well as on the rest mass of the emitted particle. For relativistic or massless particles $\Gamma_s(E, M)$ is a function of ME; its exact form has to be calculated numerically [10]. It can be adequately approximated in terms of the absorption cross section $\sigma_s(E, M)$ [8]:

$$\Gamma_s(E, M) = \frac{E^2 \sigma_s(E, M)}{\pi \hbar^2 c^2}, \tag{3}$$

where $\sigma_s(E, M)$ can be replaced by its averaged value [8]

$$\bar{\sigma}_s = \frac{\int \mathrm{d}E \ \sigma_s(E, M)}{\int \mathrm{d}E} = \begin{cases} 56.7 \ G^2 M^2/c^4 & s = \frac{1}{2} \\ 20.4 \ G^2 M^2/c^4 & s = 1 \\ 2.33 \ G^2 M^2/c^4 & s = 2 \ . \end{cases} \tag{4}$$

Particle physics determines the number of states the black hole emits at a given temperature. They can be emitted directly by the Hawking mechanism, or by the decay and fragmentation products of such particles. The first flux we will refer to as "direct", the latter as "indirect" fluxes. As a consequence of emission the black hole loses mass at a rate

$$\frac{\mathrm{d}M}{\mathrm{d}t} = -\frac{\alpha(M)}{M^2}, \tag{5}$$

where $\alpha(M)$ counts the degrees of freedom of the emitted particles. As the black hole radiates, its temperature rises at an increasing rate because $\alpha(M)$ increases smoothly at the rest mass threshold for each new massive particle [8]. For the Standard Model $\alpha(M)$ is shown in Fig. 1 of Ref. [9]. The details of the final stage of the PBH evaporation thus depend on the high energy value of $\alpha(M)$ which is determined by the underlying particle physics. Whatever the model, the black hole loses mass approximately as M^{-3}, and

its temperature increases accordingly. Its luminosity increases roughly as M^{-2} as M decreases. We will refer to this runaway process as explosion.

To a good approximation the solution of Eq. (5) for the evolution with time of the mass $M(t)$ of a black hole with initial mass M_i is

$$M(t) \simeq (M_i^3 - 3\alpha t)^{1/3} = M_* \left(\left(\frac{M_i}{M_*} \right)^3 - \frac{t}{t_0} \right)^{1/3}, \tag{6}$$

where $\alpha = \alpha(M_*)$ and t_0 is the age of the Universe. We recall that M_* is the mass of a black hole, formed in the early Universe and evaporating today. One can use Eq. (6) to relate the initial mass M_i of the black hole to the lifetime τ over which it completely evaporates.

The most conservative choice for the underlying particle physics model is the Standard Model. It provides a lower bound on the high energy value of $\alpha(M)$, not only because its degrees of freedom are restricted to known particles with the exception of the Higgs, but also because above the deconfinement temperature, $T_{_D} \sim \Lambda_{QCD} \simeq 100 - 300\ GeV$, quarks and gluons are emitted as fundamental particles instead of pions and heavier hadrons. Quarks and gluons subsequently fragment into (mostly) pions. Only pions can be emitted directly below the deconfinement temperature, assuming that their rest mass is somewhat smaller than Λ_{QCD}. Other models may include more degrees of freedom. For example supersymmetry increases $\alpha(M)$ by at least a factor of 3. Instead of trying to list all the possibilities, we only mention the other extreme example, the Hagedorn picture, where the number of degrees of freedom increases exponentially. In Hagedorn-type models spectacular explosions are obtained because of these exponentially increasing hadron degrees of freedom. We consider these models unrealistic in the framework of QCD and will not consider them further. Throughout this paper we will assume the degrees of freedom to be those of the Standard Model, even at the highest temperatures, and in our calculations we will use $T_{_D} = 200$ GeV, $m_{\rm top} = 170$ GeV and $m_{\rm Higgs} = 100$ GeV.

3 Neutrino fluxes

We are now ready to calculate the neutrino fluxes for each species. The direct neutrino flux, which is the same for all neutrino flavors, is given by Eq. (1).

The indirect neutrino fluxes are flavor dependent and fall into two categories. They can be the decay products of directly emitted heavier particles, like muons or taus. Above the QCD deconfinement temperature they can also be produced by the decay of quark and gluon fragmentation products, mostly pions in quark jets. These fluxes are studied in detail in [8]. Here we shall make the adequate approximation that all the fragmentation products are pions, hence the decay of fragmentation products only contributes to the muon and electron neutrino flux through charged pion decay.

Our main results are independent of the explicit choice of the quark fragmentation function. We use the empirical fragmentation function [11]

$$\frac{\mathrm{d}N_\pi}{\mathrm{d}z} = \frac{15}{16}(z-1)^2 z^{-3/2}, \tag{7}$$

where $z = E_\pi/E$ and E is the quark (jet) energy. This choice of the fragmentation function is convenient because it yields realistic, analytic expressions for the hadron decay fluxes when we further approximate the flux by a delta function at its peak value [9].

Two thirds of the pions are charged and decay into $\bar{\nu}_\mu + \mu$ and their charge conjugates. The direct quark emission is convoluted with the fragmentation function and the pion decay distributions. Naturally, whenever fragmentation is considered, the flux depends on the PBH mass at the moment of emission. The muons from pion decay also decay ($\mu^- \rightarrow \nu_\mu\ \bar{\nu}_e\ e^-$), and thus contribute to the ν_μ and the ν_e fluxes. To calculate the contributions of such decays the convolution must therefore also involve muon decay.

The decay distribution of a particle from any decay is given by:

$$\frac{\mathrm{d}n}{\mathrm{d}E} = \frac{1}{\Gamma}\frac{\mathrm{d}\Gamma}{\mathrm{d}E}\ , \tag{8}$$

where Γ is the decay width. The distribution is normalized to the number of identical particles produced by a single decay. The calculations are straightforward. Below we explicitly list the distributions used because they correct errors in an earlier calculation [8]:

Pion decay: $\pi^\pm \ \rightarrow\ \mu^\pm\ \nu_\mu(\bar{\nu}_\mu)$. The ν_μ distribution is given by:

$$\frac{dn_{\nu_\mu}}{\mathrm{d}E_\nu} = \delta\left(E_\nu - (\frac{m_\pi^2 - m_\mu^2}{2m_\pi})\right), \tag{9}$$

in the rest frame of the pion ($\beta = 0$), and

$$\frac{dn_{\nu_\mu}}{\mathrm{d}E_\nu} = \frac{m_\pi^2}{m_\pi^2 - m_\mu^2} \frac{1}{\sqrt{E_\pi^2 - m_\pi^2}} \ , \tag{10}$$

where the allowed range of E_ν is

$$\frac{\frac{1}{2}\left(m_\pi^2 - m_\mu^2\right)}{E_\pi + \sqrt{E_\pi^2 - m_\pi^2}} \leq E_\nu \leq \frac{\frac{1}{2}\left(m_\pi^2 - m_\mu^2\right)}{E_\pi - \sqrt{E_\pi^2 - m_\pi^2}} \tag{11}$$

in the lab frame ($\beta \neq 0$).

Muon decay: $\mu^\pm \to \bar{\nu}_\mu(\nu_\mu)\ \nu_e(\bar{\nu}_e)\ e^\pm$ The distribution of the muon neutrinos is given by:

$$\frac{\mathrm{d}n_{\nu_\mu}}{\mathrm{d}E_\nu} = \frac{2}{\gamma m_\mu} \times \begin{cases} \frac{1}{\beta}\left[\frac{5}{6} - \frac{3}{2}\epsilon^2 + \frac{2}{3}\epsilon^3\right] & \text{for } \frac{1-\beta}{1+\beta} \leq \epsilon \leq 1 \ , \\ 2\left(1+\beta\right)^2\left[3\epsilon^2 - \frac{2}{3}\left(\frac{3+\beta^2}{1-\beta}\right)\epsilon^3\right] & \text{for } 0 \leq \epsilon \leq \frac{1-\beta}{1+\beta} \ . \end{cases} \tag{12}$$

Similarly the electron neutrino distribution is:

$$\frac{\mathrm{d}n_{\nu_e}}{\mathrm{d}E_\nu} = \frac{2}{\gamma m_\mu} \times \begin{cases} \frac{1}{\beta}\left[1 - 3\epsilon^2 + 2\epsilon^3\right] & \text{for } \frac{1-\beta}{1+\beta} \leq \epsilon \leq 1 \ , \\ 4\left(1+\beta\right)^2\left[3\epsilon^2 - \left(\frac{3+\beta^2}{1-\beta}\right)\epsilon^3\right] & \text{for } 0 \leq \epsilon \leq \frac{1-\beta}{1+\beta} \ . \end{cases} \tag{13}$$

In both the above cases $\epsilon = E_\nu / E_\nu^{\max}$, where

$$E_\nu^{\max} = \frac{\gamma m_\mu}{2}(1+\beta), \tag{14}$$

is the maximum neutrino energy, and the electron mass is neglected.

Tau neutrinos represent a somewhat different story. They can hardly be produced in hadron decays since decays of hadrons into ν_τ are highly suppressed. Decays into $\nu_\tau\ \bar{\nu}_\tau$ proceed via Z^0 exchange and therefore are suppressed with respect to decays mediated by a photon. Decays into a $\tau - \nu_\tau$ or $\tau - \bar{\tau}$ pairs are kinematically forbidden except for heavy hadrons which rarely appear as quark or gluon fragmentation products. Moreover, the decays into $\tau - \nu_\tau$ channels have small branching ratios. In the end most of the ν_τ flux is direct. The only other significant contribution comes from the decay of direct τ's.

For the neutrino fluxes from τ decay we estimate that $\sim 40\%$ of the decays occur in leptonic modes, with the rest in semi-hadronic modes. In the free quark approximation this comes from the relative number of colors (3) to neutrino flavors (2) into which the decay may proceed. The number distributions for each type of particle are the same as the above three body distribution in the limit of massless final states. Thus an approximate ν_τ flux is given by replacing m_μ by m_τ in the above formulas. The ν_e and ν_μ fluxes coming from $\tau \to e\bar{\nu}_e\nu_\tau$ and $\tau \to \mu\bar{\nu}_\mu\nu_\tau$, respectively, are each 20% of the total ν_τ flux from τ decay.

In the following sections we will compute $f(x, M)$, the total neutrino flux of energy $E = (8\pi GM/\hbar c^3)^{-1} x$ for a given species. For ν_μ, the direct, the muon decay, and the fragmentation flux contribute to $f(x, M)$. The direct flux depends on x only, while the fragmentation flux depends also on the PBH mass M at the time of the emission.

4 Diffuse neutrino fluxes

Our calculation of the diffuse neutrino spectrum closely parallels that of Ref. [2] for gamma rays. In order to calculate the present neutrino flux of energy E_0 we must integrate the contributions over cosmological time t for all PBH of mass M at the blue shifted energy E

$$E = \frac{E_0}{r}, \tag{15}$$

where $r \equiv R/R_0 = (1 + Z)^{-1}$, Z is the redshift at time t. The subscript 0 denotes the value of a quantity at the present epoch. We assume a standard Friedman cosmological model. Thus the Universe is radiation dominated for $t < 10^{-6}$ s and matter dominated for $t > 10^{-6}$ s.

Assuming a uniform distribution of PBHs, created shortly after $t = 0$, the initial number of PBHs per comoving volume of mass less than M_i is

$$n(M_i) \equiv \mathcal{N} \int_0^{M_i/M_*} \mathrm{d}y \; s(y) \; , \tag{16}$$

where $y = M_i/M_*$ and $s(y)$ is a dimensionless function that determines the form of the initial mass distribution. Here $s(1) = 1$. $\mathcal{N}$ is the initial number density of PBH per logarithmic mass interval at $M = M_*$. From various

cosmological considerations we know that $\mathcal{N} \leq 10^4\ pc^{-3}$. PBH clustering in the galaxy can increase their local density by as much as a factor of $\xi = 10^7$ which dramatically improves our chances to observe them [9]. In our calculations we will not assume any clustering, *ie.* $\xi = 1$.

If PBHs form from scale invariant density perturbations with a Gaussian spectrum, then

$$s(y) = y^{-\beta}, \tag{17}$$

where $2 < \beta < 3$, depending on the equation of state of the Universe at the formation of PBHs [3]. If $p = \gamma\rho$, where p is the presure and ρ is the energy density, then

$$\beta = \frac{1+3\gamma}{1+\gamma} + 1\ . \tag{18}$$

Let $f(x, M)$ represent the total neutrino flux of energy E_ν as defined in the previous section, then the diffuse flux per unit area today is:

$$\frac{d^4N_\nu}{dA\ d\Omega\ dt\ dE_{\nu 0}} = \frac{\mathcal{N}c}{4\pi}\int_0^{t_0} \mathrm{d}t'(1+Z)\int \mathrm{d}y\ s(y)\ f(x,M)\ , \tag{19}$$

where y is to be integrated over all values of the initial masses of the PBHs present at t', and x is the value of $(8\pi GM/\hbar c^3)\, E_\nu$ at t' and y. Absorption on ambient matter in the Universe should be taken into account. For neutrinos this is negligible. Making use of (6) and (17), the integral (19) becomes:

$$\begin{aligned}\frac{d^4N_\nu}{dA\ d\Omega\ dt\ dE_{\nu 0}} &= \frac{\mathcal{N}c}{4\pi x_*^3}\int_0^1 dt'\ r^2\int_0^\infty dx\ x^2 \\ &\quad \times f(x,M)\left(\frac{t'}{t_0}+\frac{r^3x^3}{x_*^3}\right)^{-(\frac{\beta+2}{3})}\ ,\end{aligned} \tag{20}$$

where $x_* = (8\pi GM_*/\hbar c^3)\, E_\nu$. The right hand side can be integrated numerically once the contributions to $f(x, M)$ are specified. For electron neutrinos we include the contribution from the decay of secondary muons (from the decay of fragmentation pions), the decay of direct muons and taus and the direct flux. For muon neutrinos we include the contributions from the decay of fragmentation pions, the decay of secondary muons, the decay of direct muons and taus and the direct flux. In the fragmentation case the

x-integration limits are modified. For tau neutrinos only the direct flux and the flux from direct tau decay contribute significantly as discussed earlier.

In Figs. 1 and 2 we plot the resulting fluxes. The fluxes have been calculated for a PBH density taken to be the maximum allowed by bounds derived from gamma ray measurements [9]. The main characteristics of the neutrino fluxes are: i) in the low energy region the slopes of the curves are β dependent, while at high energies they decrease as E^{-3}, independent of β, ii) all fluxes display a "knee" (a change of slope) in the 50-100 MeV region corresponding to the peak emission energy of black holes of mass M_*, iii) the fragmentation spectra display a knee at around 10 MeV and, finally, iv) the direct spectra are negligible above the knee and dominate in the region below.

5 Background fluxes and bounds on PBH abundances

It is in principle possible to obtain an improved bound whenever the predicted neutrino fluxes, computed for the maximal PBH abundance allowed by the gamma-ray bound, exceed the neutrino backgrounds. These are predominantly of solar and atmospheric origin and can be separated by energy region.

The solar flux extends to 18.8 MeV where it is sharply cut off. Below the cutoff it dominates with a very featured spectrum which traces the different nuclear reactions in the Sun's interior. The reaction yielding the lowest flux but the most energetic neutrinos is $He + p \rightarrow \nu_e + \ ...$, usually abbreviated *hep*. This flux is large compared to the diffuse PBH flux but it has two distinguishing characteristics that can be used to suppress it: i) it is of ν_e flavor and ii) directional. The required rejection rate of order $10^{-6} - 10^{-9}$ is challenging in spite of the excellent sensitivity of the detectors to the neutrino direction, especially for the *hep* and ^7B fluxes. Flavor identification at this level seems difficult since ν_μ or ν_τ are not detected. Finally, flavor identification is only valid in the absence of solar flavor oscillations, an issue which is unsettled.

Above the solar cutoff the background neutrinos fluxes are dominated by the decays of hadrons produced by interactions of cosmic rays with atmo-

spheric nuclei. The main contribution is from pions with $\nu_e : \nu_\mu \simeq 1 : 2$. The atmospheric neutrino fluxes are understood with roughly 10% precision. At the lower energies they are strongly dependent on the magnetic latitude and arrival directions because of the geomagnetic cutoff for cosmic rays. Locations with low geomagnetic latitude have smaller atmospheric neutrino fluxes at low energies which is an advantage if a bound on PBHs is to be extracted.

The atmospheric flux of ν_τ is multiply suppressed. The open decay channels involve heavy parents such as D_s or bottom hadrons [12] which have smaller production cross section than pions and kaons and branching ratios for $\nu_\tau\tau$ decays which are over an order of magnitude (4% for D_s) below those for pions and kaons. Production of heavy hadrons has a higher threshold energy. Because of the steepness of the cosmic ray parent flux, increased thresholds result in a drastic suppression of the flux at low energies. The calculation is very similar to that of the prompt muon neutrino flux of charm origin [13] and subject to similarly large uncertainties associated with our poor understanding of the production cross section for D_s in the region near threshold. There is no point then in performing a detailed calculation, and we obtain a simple estimate of the ν_τ flux by rescaling the prompt muon flux by a factor. Considering that D_s production is suppressed and that the branching ratios of the decays $D_s \to \nu_\tau + ...$ are smaller than the corresponding ones for the decays of other Ds, we approximate the above factor to be of order 0.1. This agrees with the estimates made for LHC [14].

In Fig. 3 we compare PBH fluxes to the atmospheric ν_e and ν_μ fluxes at a north U.S. location [21], to the solar neutrino *hep* flux and to our estimate of the atmospheric ν_τ flux. The PBH fluxes are calculated for $\beta = 3$, because one can assume that at the formation of PBHs the Universe is radiation dominated. The figure allows one to identify the most promising regions for obtaining an improved bound. The high energy region is promising since the background falls faster than the signal. Unfortunately prompt neutrinos from charm decay are expected to dominate at the highest energies over the fluxes of pion and kaon decay origin and may thus prevent the atmospheric neutrino flux to fall below the PBH flux. On a more speculative note, the high energy neutrino flux may be dominated by point sources which is not a problem unless a large number conspire to produce a diffuse flux. Searching for a ν_τ flux seems to be most promising. Even nonobservation is of interest as it may yield important bounds on PBH abundances.

6 Final stage evolution: detection of ν's from individual black holes

As we have seen in Sect. 2 the final stage of a PBH is explosive. In order to determine the present density of these exploding black holes one must look for individual sources. In this section we show that high energy neutrino telescopes can significantly contribute to this search. Their threshold energy is of order $E \geq 10\ GeV$ for ν_μ neutrinos. The main contribution to the flux $f(x, M)$ comes, in the case of explosions, from the decay of fragmentation pions. This is because other contributions are either smaller or peak at lower energies.

Because we are going to consider PBHs whose lifetimes are short compared to a typical observation time (of order of years), the relevant quantity is the time integrated flux

$$\begin{aligned} \frac{\mathrm{d}N_\nu}{\mathrm{d}E} &= \int_{t_i}^{t_f} \mathrm{d}t f(x, M) \\ &= 1.19\ 10^{39} GeV^{-1} \left(\frac{1GeV}{E}\right)^3 \int_0^{E/kT_i} \mathrm{d}x x^2 \alpha^{-1} f(x, M), \end{aligned} \tag{21}$$

where $x = E/kT$. Here we have used Eqs. (2) and (5) to convert the time integral into an integral over the inverse temperature. We can neglect redshift effects because we will find that one does not expect to see PBH explosions from further than a few parsecs.

The ν_μ's interact with the Earth and the secondary upcoming muons produce the experimental signature in the underground detector. Only muons entering the detector from below are detected, because the background of downward atmospheric muons dominates any neutrino-induced signal. The probability that a neutrino produces a muon above the threshold energy E_D at the detector [15] is

$$P_{\nu\to\mu}(E_\nu, E_D) = N_A \int_{E_D}^{E_\nu} dE_\mu \frac{\mathrm{d}\sigma}{\mathrm{d}E_\mu}(E_\mu, E_\nu) R_\mu(E_\mu, E_D), \tag{22}$$

where N_A is Avogadro's number, $\mathrm{d}\sigma/\mathrm{d}E_\mu$ is the differential charged current cross section [18, 19] and R_μ is the muon range [16]. We updated $\mathrm{d}\sigma/\mathrm{d}E_\mu$ of [18, 19] by using the latest small-x parton distribution functions of [20].

The evaluation of Eq. (22) was carried out using the Monte Carlo integration routine VEGAS [17].

The predictions relevant to experiment are obtained by integrating the muon flux in the detector above E_D. The number of observed events is given by:

$$N_\nu(E_D,\theta) = \frac{A}{4\pi r^2}\int_{E_D}^{\infty} \mathrm{d}E\ P_{\nu\to\mu}\exp\left[-\sigma_{\rm tot}(E_\nu)N_A X(\theta)\right]\frac{\mathrm{d}N_\nu}{\mathrm{d}E}, \tag{23}$$

where r is the distance to the PBH, A is the sensitive area of the detector, the exponential factor accounts for absorption of neutrinos along the chord of the Earth $X(\theta)$ and $\sigma_{\rm tot}$ is the total cross section [19]. Here θ is the zenith angle ($0 \le \theta \le 90^\circ$). The dominant contribution to the integral (23) comes from and is evaluated for nearly vertical neutrinos ($\theta \simeq 0$), because only neutrinos with small θ travel far enough in the Earth to interact and produce a muon. Detectors under construction may, eventually, reach an effective area of order $A \simeq 1$ km^2. The threshold energy can be anywhere between a few GeV to a few TeV.

Because the number of events is inversely proportional to r^2, there is a maximum r for which the PBH is detectable. This distance depends on the initial temperature of the PBH and is increased for lower temperatures because of the increased observation time. Fig. 4 shows this maximum distance as a function of the detector threshold energy E_D for initial temperatures ranging from 50 GeV to 20 TeV. The limiting distance is determined by the requirement that we detect at least 10 muons per burst.

For a PBH to be detectable it has to stand out over background. In this case the high energy atmospheric flux is the relevant background. Our calculation follows Ref. [22], and is in agreement with other calculations and measurements of the atmospheric neutrino background [21]. The number of background events in the detector is:

$$N_{\rm bgr} = \tau\ A\int_{E_D}^{\infty}\mathrm{d}E\ \omega_D(E)\ \frac{\mathrm{d}^4\ N}{\mathrm{d}A\ \mathrm{d}t\ \mathrm{d}\omega\ \mathrm{d}E}\ P_{\nu\to\mu}\ , \tag{24}$$

where ω_D is the angular resolution of the detector

$$\omega_D(E) = \frac{0.314\ \mathrm{sr}}{E(\mathrm{GeV})}\ , \tag{25}$$

and τ is the lifetime of the black hole. For detectability we require that the signal (23) exceeds the background (24) by 5σ. The maximum distance for which this condition holds, is shown on Fig. 4 as a function of the detector energy for initial temperatures ranging from 50 GeV to 20 TeV.

The distance of an observable PBH must fall below both curves on Fig. 4. For $kT_i \geq 1$ TeV the 10 muon signal condition is stronger. This is because the lifetime of such a PBH is so short that few background events can accumulate during its observation. For lower initial temperatures the 10 muon signal condition is stronger for high detector thresholds, while the 5σ condition is stronger for low thresholds. This combined condition is shown on Fig. 5. The optimal condition is obtained for a PBH with $kT_i \simeq 100$ GeV. The lifetime of such a PBH is about 1.5 months, longer than the lifetime of PBHs usually referred as "explosive" in the literature, but still small compared to the detection time. The maximum distance is 2.3×10^{-3}pc at $E_D \simeq 140$ GeV, which gives an upper bound $1.2 \times 10^7 \mathrm{pc}^{-3}\mathrm{yr}^{-1}$ on the number of PBHs exploding in our neighborhood per year. Here we used detector solid acceptance angle 2π, observational time 3.3 years, and assumed a uniform PBH distribution in our neighborhood. The detector acceptance solid angle is 2π because only upward muons have experimental signature. In order to compare our result to existing experimental bounds, we choose the observation time to be that of the search establishing the strongest bound. It is $8.5 \times 10^5 \mathrm{pc}^{-3}\mathrm{yr}^{-1}$ from high energy γ ray measurement from $kT_i \simeq 10$ TeV PBH, and it is of two order of magnitude smaller than that of any other direct search [23].

Our result is stronger than any existing experimental bounds, except that of [23]. Our bound is about an order of magnitude larger, but can be interesting if for some reason detection of neutrinos is preferable over detection of γ rays from PBHs. The issue has indeed been raised whether γ rays are emitted as independent particles in the presence of thermal electrons surrounding the black hole [24].

7 Detector considerations

It obviously remains to be seen whether detectors will ever reach the sensitivities to observe the neutrino fluxes predicted in our calculations. In the diffuse case, the challenge is formidable as can be seen from Fig. 3. One must improve on the sensitivity to detect atmospheric neutrinos by over three orders

of magnitude even when restricting observations to the favorable vertical neutrinos. The most promising search involves tau neutrinos with energy below 10 GeV. Detecting the τ-lepton emerging from a charged current interaction may be possible since the neutrino energy can exceed the τ-lepton mass but this will certainly represent a challenge. Alternatively one may look for the difference between the total neutrino flux and those of electron and muon flavor. This procedure requires a precision of 0.1% which is probably out of question in the near future. The search for explosions presents us, in the end, with the most realistic opportunities.

8 Conclusion

In this paper we have calculated the neutrino fluxes from PBHs and their detectability for both low and high energies. We have updated the previous calculations by including contributions not only from direct neutrino emission, but from muon and tau decays and from quark fragmentation. The latter is especially important because of the large number of quark degrees of freedom.

In the diffuse case the fluxes are increasing functions of β in the allowed range $2 \leq \beta \leq 3$. The ν_μ and ν_e fluxes are dominated by the fragmentation contribution for E_ν less than about 100 MeV. Around 1 MeV it is about an order of magnitude higher than the other contributions. For larger energies all contributions decrease as E_ν^{-3}, and the total flux is dominated by the direct emission of neutrinos. In the case of ν_τ the direct flux dominates at all energies, because there is no relevant fragmentation contribution. In the individual PBH case the time integrated flux is relevant. The ν_μ contribution from the first decay of fragmentation pions is the largest.

We have compared the calculated fluxes to the relevant background to determine which neutrino species at what energy range has large enough flux to be detectable. In the diffuse case the ν_e and ν_μ fluxes are larger than the atmospheric background only for E_ν smaller than a few MeV. For ν_e the huge directional solar *hep* background can cause further observational difficulties. Most promising is the ν_τ case, because the only relevant background, the atmospheric ν_τ flux, is highly suppressed.

Our best chance is to look for individual PBHs in our neighborhood. We have shown that the new kilometer-scale, high energy ($E_D \simeq 1$ GeV $-$

1 TeV) neutrino telescopes can play a significant role in this search. They are sensitive to ν_μ's. Furthermore at these high energies the only background, the atmospheric neutrino background, is suppressed. The bound that can be established with these detectors is comparable to existing experimental bounds, obtained by searching for high energy γ ray bursts.

Acknowledgements

We thank Jesus Armada for his contribution to the early stages of this work, Ricardo Vazquez and Brian Wright for interesting discussions and Brian Wright for careful reading of the manuscript. This work was supported in part by the University of Wisconsin Research Committee with funds granted by the Wisconsin Alumni Research Foundation, in part by the U.S. Department of Energy under Contract No. DE-AC02-76ER00881, in part by the Texas National Research Laboratory Commission under Grant No. RGFY9173 and in part by the Xunta de Galicia, reseach contract XUGA 20604A93.

References

[1] S. W. Hawking, Nature (London) **248**, 30 (1974); S. W. Hawking, Commun. Math. Phys. **43**, 199 (1975).

[2] D. N. Page and S. W. Hawking, Astrophys. J. **206** , 1 (1976).

[3] B. J. Carr, Astrophys. J. **201**, 1 (1975).

[4] B. J. Carr, Astrophys. J. **206**, 8 (1976).

[5] B. J. Carr in *Observational and Theoretical Aspects of Relativistic Astrophysics and Cosmology* (eds. J. L. Sanz, *et. al.*), p.1 (World Scientific, Singapore, 1985); S. W. Hawking, Mon. Not. R. Astr. Soc. **152**, 75 (1971).

[6] S. W. Hawking, I. G. Moss and J. M. Steward , Phys. Rev. **D26**, 2681 (1982).

[7] S. W. Hawking, Phys. Lett. **B231**, 237 (1989).

[8] J. H. MacGibbon and B. R. Webber, Phys. Rev. **D41**, 3052 (1990); J. H. MacGibbon, Phys. Rev. **D44**, 376 (1991).

[9] F. Halzen, E. Zas, J. H. MacGibbon and T. C. Weeks, Nature **353**, 807 (1991).

[10] D. N. Page, Phys. Rev. **D13**, 198 (1976).

[11] C. T. Hill, D. V. Schramm and T. P. Walker, Phys. Rev. **D36**, 1007 (1987).

[12] M. Talebzadeh *et. al.* , Nucl. Phys. B291, 503 (1987).

[13] L. V. Volkova, Nuovo Cimento **C10**, 465 (1987).

[14] A. de Rújula, E. Fernandez, J. J. Gomaz-Cadenas, Nucl. Phys. **B405**, 80 (1993).

[15] T. K. Gaisser and A. F. Grillo, Phys. Rev. **D36**, 2752 (1987); T. K. Gaisser and T. Stanev, Phys. Rev. **D31**, 2770 (1985); T. K. Gaisser, F. Halzen and T. Stanev, Physics Reports (in press).

[16] P. Lipari and T. Stanev, Phys. Rev. **D44**, 3543 (1991).

[17] G. P. Lepage, J. Comput. Phys. **27**, 192 (1978); W. H. Press, *et. al.*, *Numerical Recipes* (Cambridge University, Cambridge, second edition).

[18] D. W. McKay and J. P. Ralston, Phys. Lett. **167B**, 103 (1986); C. Quigg, M. H. Reno and T. P. Walker, Phys. Rev. Lett. **57**, 774 (1986).

[19] M. H. Reno and C. Quigg, Phys. Rev. **D37**, 657 (1988).

[20] A. D. Martin, W. J. Stirling and R. G. Roberts, preprints RAL-94-055, DTP/94/34 and RAL-94-104, DTP/94/78.

[21] T. K. Gaisser, T. Stanev and G. Barr, Phys. Rev. **D38**, 85 (1988), and references therein.

[22] L. V. Volkova, Yad. Fiz. **31**, 1510 (1980) [Sov. J. Nucl. Phys. **31**, 784 (1980)].

[23] D. E. Alexandreas *et. al.*, Phys. Rev. Lett. **71**, 2524 (1993), and references therein.

[24] A. Heckler, private communications.

Figure captions

Fig. 1. Contributions to diffuse neutrino flux (a) for ν_e, (b) for ν_μ and (c) for ν_τ.

Fig. 2. Total diffuse neutrino fluxes for β= 2, 2.5 and 3 and (a) for ν_e, (b) for ν_μ and (c) for ν_τ.

Fig. 3. Total diffuse neutrino fluxes for β=3 compared to the atmospheric neutrino backgrounds and to the solar *hep* flux.

Fig. 4. The 10 muon signal (dotted lines) and 5σ signal (solid lines) conditions as the function of the detector threshold energy, $E_{_D}$. Dotted lines correspond to kT_i = 50 GeV, 100 GeV, 200 GeV, 500 GeV, 1 TeV, 2 TeV, 5 TeV, 10 TeV and 20 TeV from top to bottom, solid lines correspond to the same kT_i values from bottom to top.

Fig. 5. Combined 10 muon signal and 5σ signal conditions as the function of the detector threshold energy $E_{_D}$ for kT_i = 50 GeV, 100 GeV, 150 GeV, 200 GeV, 500 GeV, 1 TeV, 2 TeV, 5 TeV, 10 TeV and 20 TeV.

Figure 1 (a)

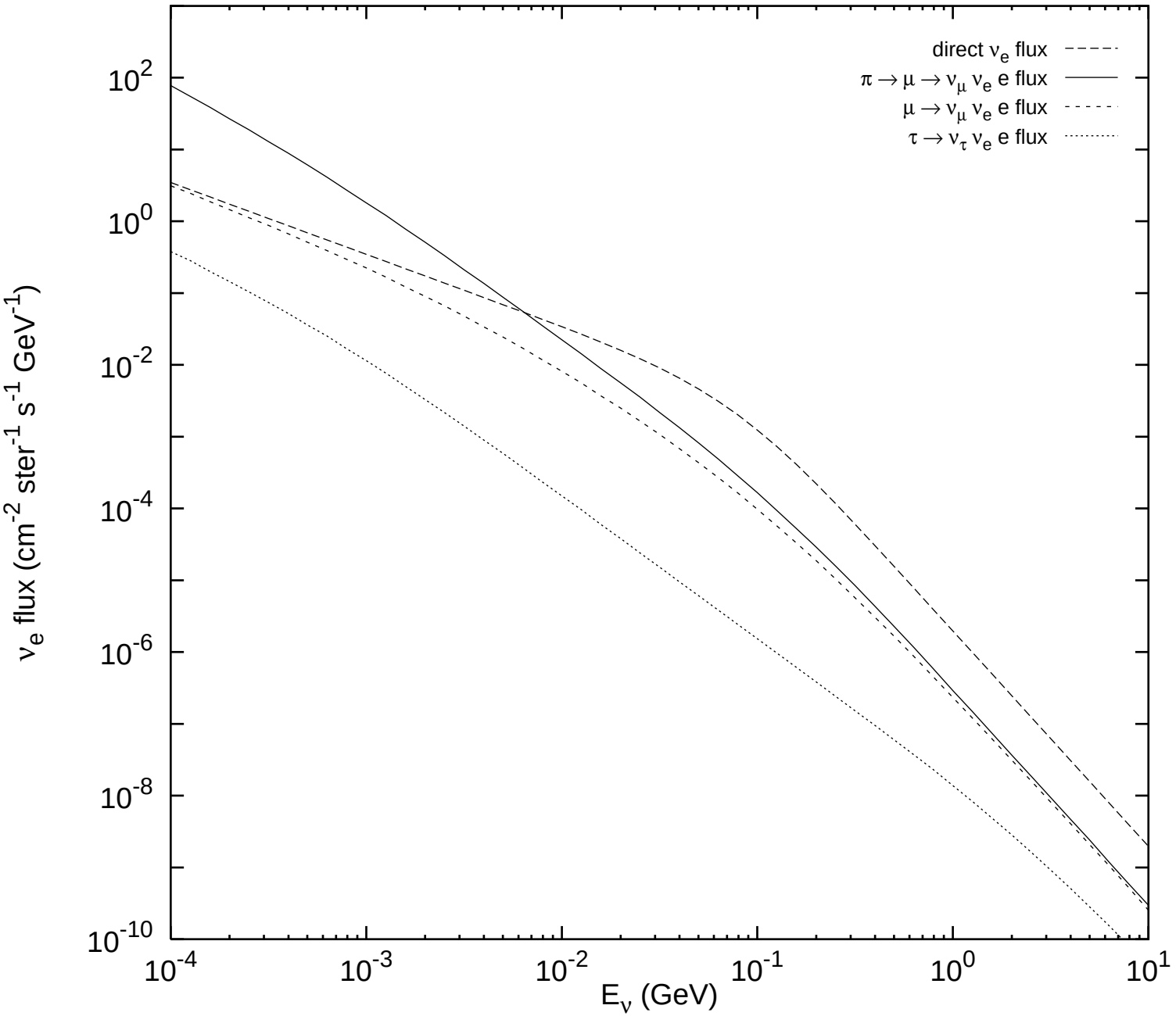
direct ν_e flux
$\pi \rightarrow \mu \rightarrow \nu_\mu\ \nu_e$ e flux
$\mu \rightarrow \nu_\mu\ \nu_e$ e flux
$\tau \rightarrow \nu_\tau\ \nu_e$ e flux
ν_e flux (cm^{-2} ster^{-1} s^{-1} GeV^{-1})
E_ν (GeV)
10^{2}
10^{0}
10^{-2}
10^{-4}
10^{-6}
10^{-8}
10^{-10}
10^{-4}
10^{-3}
10^{-2}
10^{-1}
10^{0}
10^{1}

Figure 1 (b)

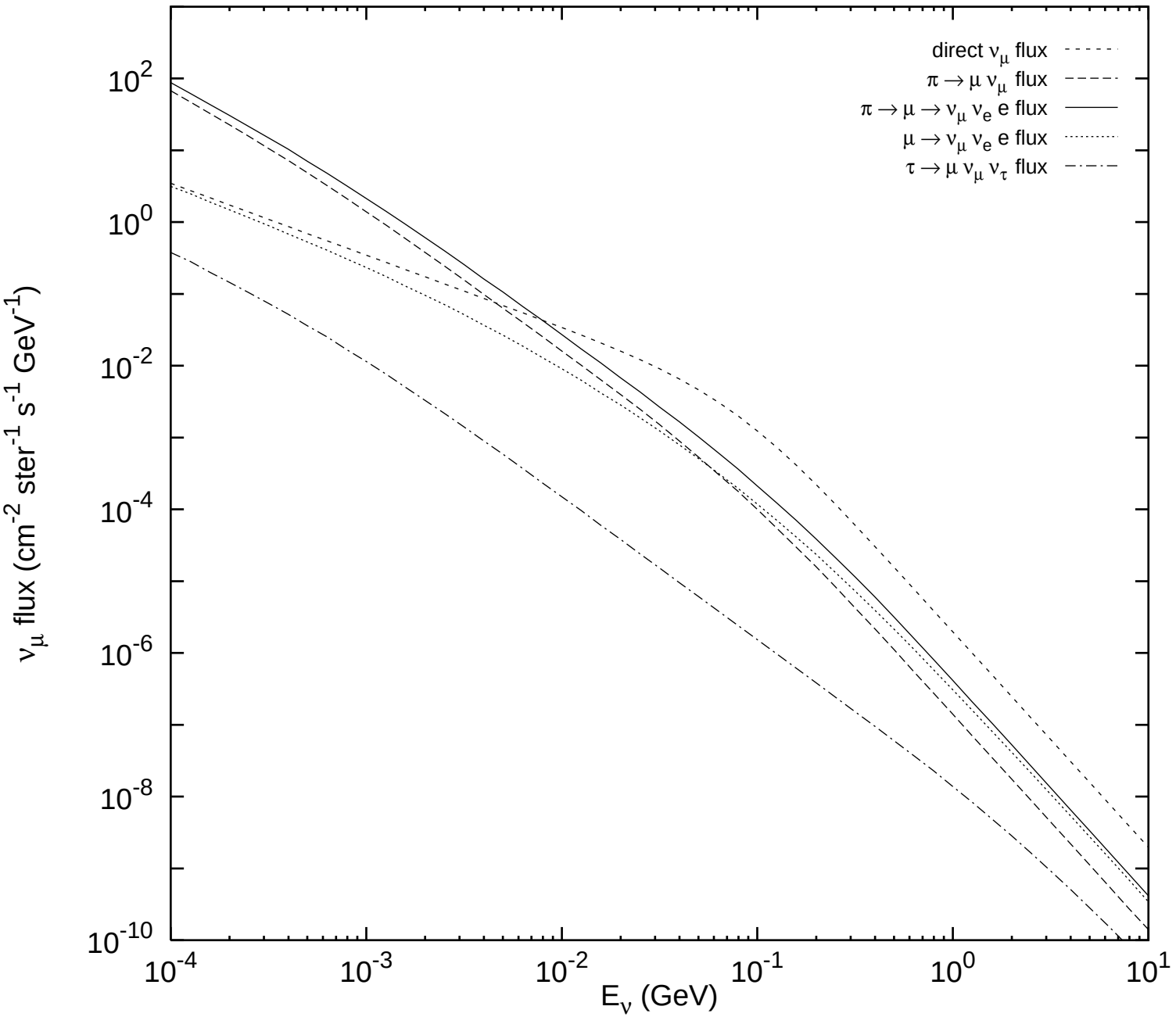
direct ν_μ flux
$\pi \rightarrow \mu\ \nu_\mu$ flux
$\pi \rightarrow \mu \rightarrow \nu_\mu\ \nu_e$ e flux
$\mu \rightarrow \nu_\mu\ \nu_e$ e flux
$\tau \rightarrow \mu\ \nu_\mu\ \nu_\tau$ flux
ν_μ flux (cm^{-2} ster^{-1} s^{-1} GeV^{-1})
E_ν (GeV)
10^{2}
10^{0}
10^{-2}
10^{-4}
10^{-6}
10^{-8}
10^{-10}
10^{-4}
10^{-3}
10^{-2}
10^{-1}
10^{0}
10^{1}

Figure 1 (c)

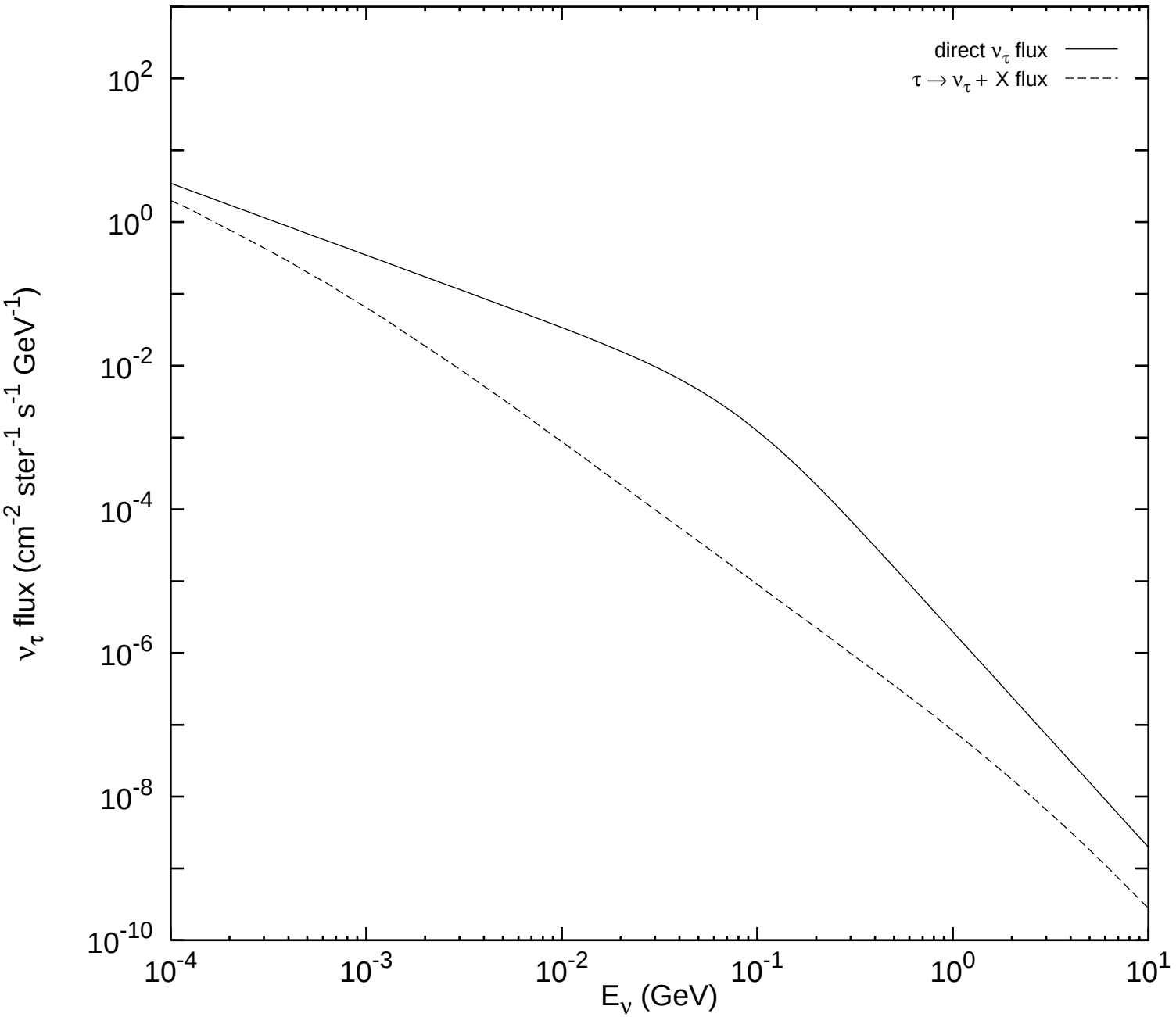
direct ν_τ flux
$\tau \rightarrow \nu_\tau$ + X flux
ν_τ flux (cm^{-2} ster^{-1} s^{-1} GeV^{-1})
E_ν (GeV)
10^{2}
10^{0}
10^{-2}
10^{-4}
10^{-6}
10^{-8}
10^{-10}
10^{-4}
10^{-3}
10^{-2}
10^{-1}
10^{0}
10^{1}

This figure "fig1-1.png" is available in "png" format from:

http://arxiv.org/ps/hep-ph/9502268v1

Figure 2 (a)

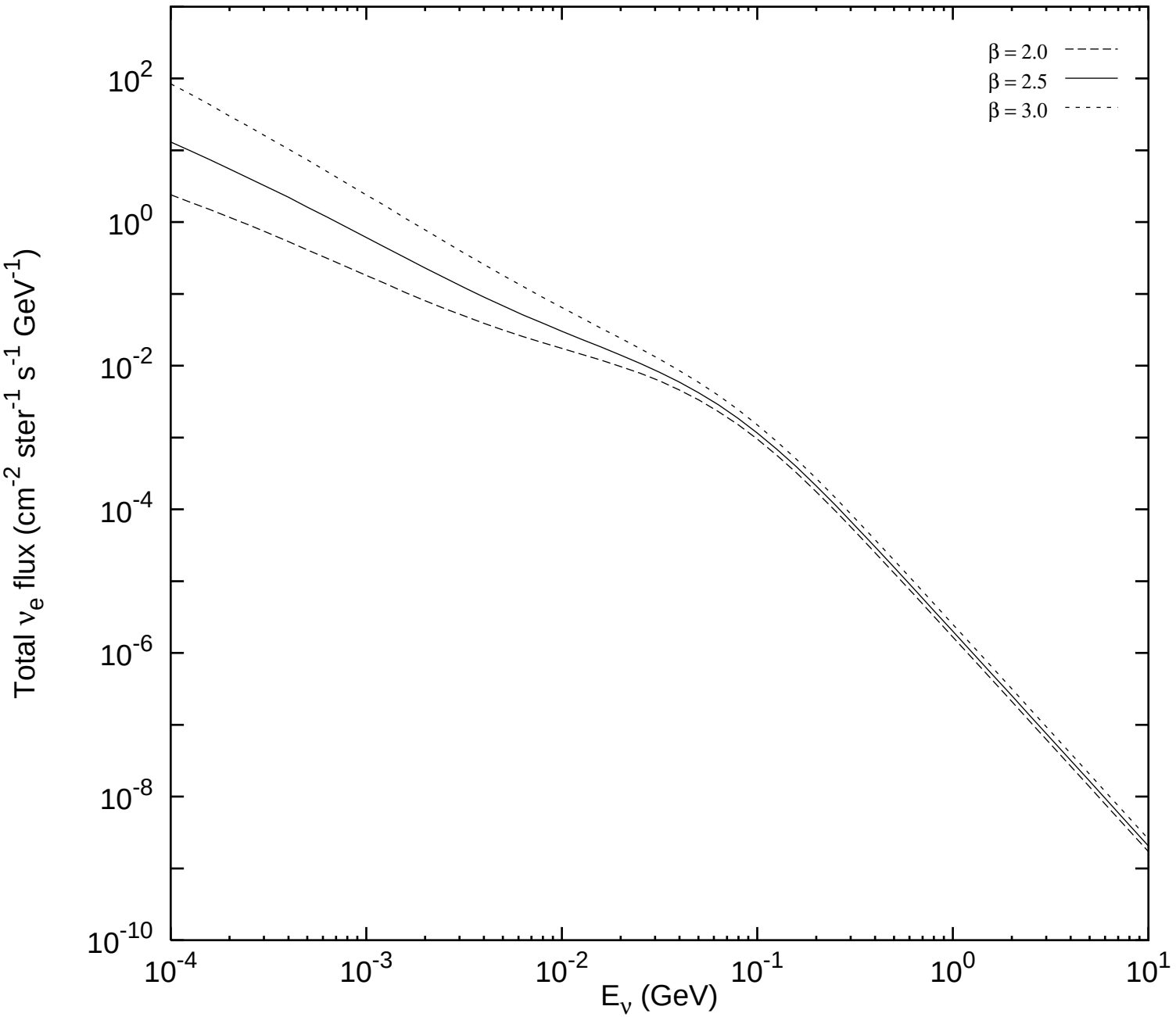
β = 2.0
β = 2.5
β = 3.0
Total ν_e flux (cm^{-2} ster^{-1} s^{-1} GeV^{-1})
E_ν (GeV)
10^{2}
10^{0}
10^{-2}
10^{-4}
10^{-6}
10^{-8}
10^{-10}
10^{-4}
10^{-3}
10^{-2}
10^{-1}
10^{0}
10^{1}

Figure 2 (b)

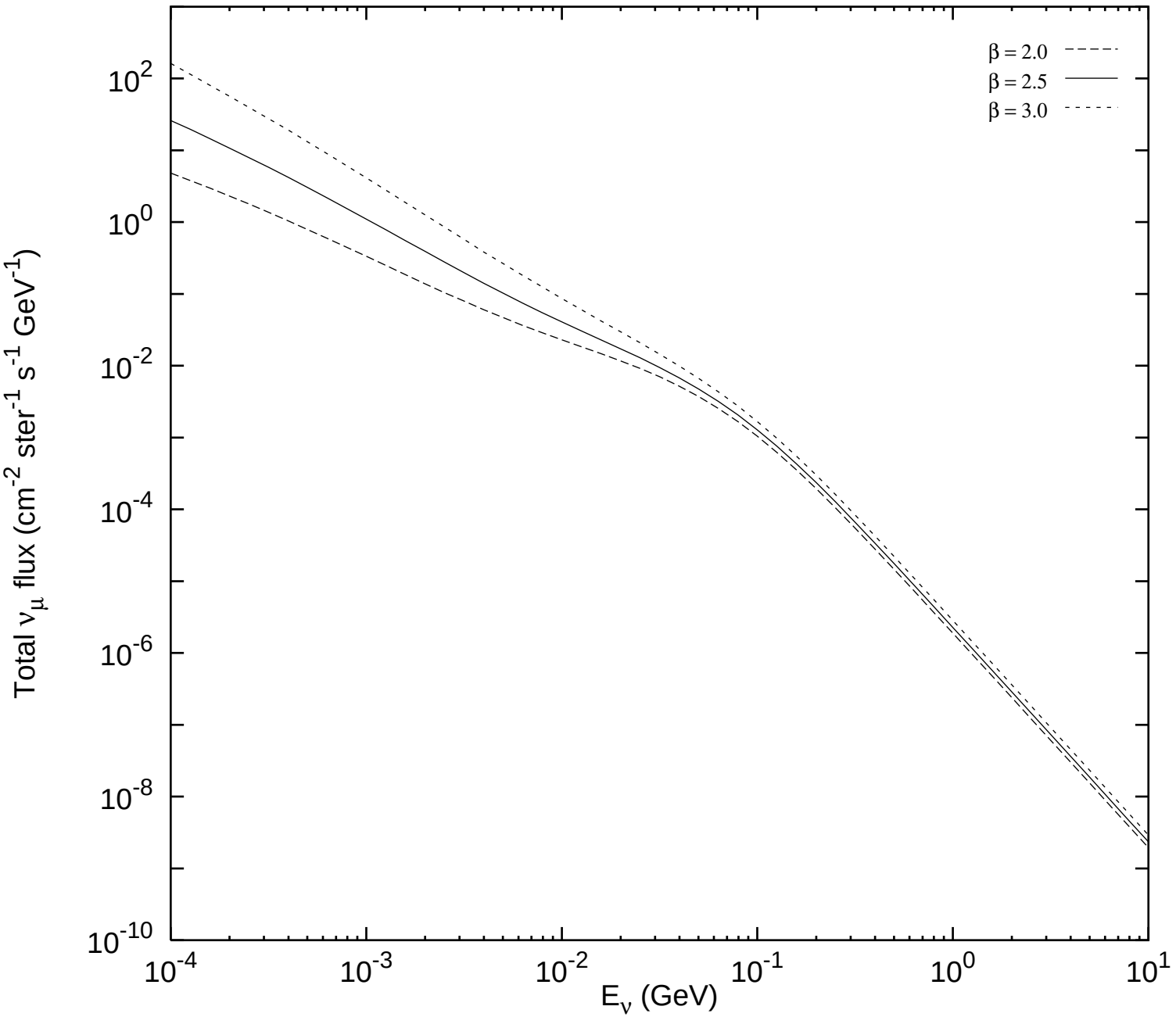
β = 2.0
β = 2.5
β = 3.0
Total ν_μ flux (cm^{-2} ster^{-1} s^{-1} GeV^{-1})
E_ν (GeV)
10^{2}
10^{0}
10^{-2}
10^{-4}
10^{-6}
10^{-8}
10^{-10}
10^{-4}
10^{-3}
10^{-2}
10^{-1}
10^{0}
10^{1}

Figure 2 (c)

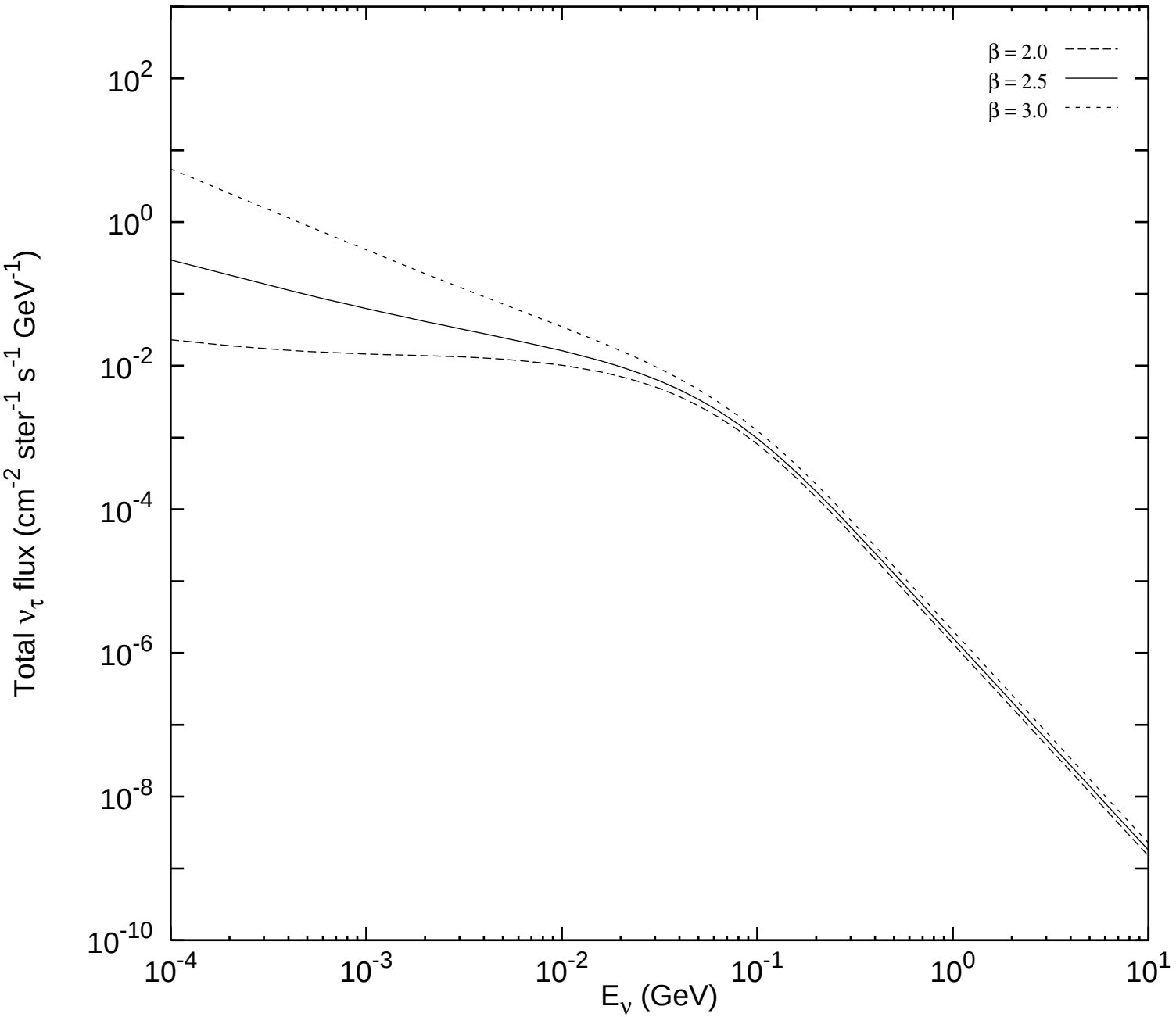
β = 2.0
β = 2.5
β = 3.0
Total ν_τ flux (cm^{-2} ster^{-1} s^{-1} GeV^{-1})
E_ν (GeV)
10^{2}
10^{0}
10^{-2}
10^{-4}
10^{-6}
10^{-8}
10^{-10}
10^{-4}
10^{-3}
10^{-2}
10^{-1}
10^{0}
10^{1}

This figure "fig1-2.png" is available in "png" format from:

http://arxiv.org/ps/hep-ph/9502268v1

Figure 3

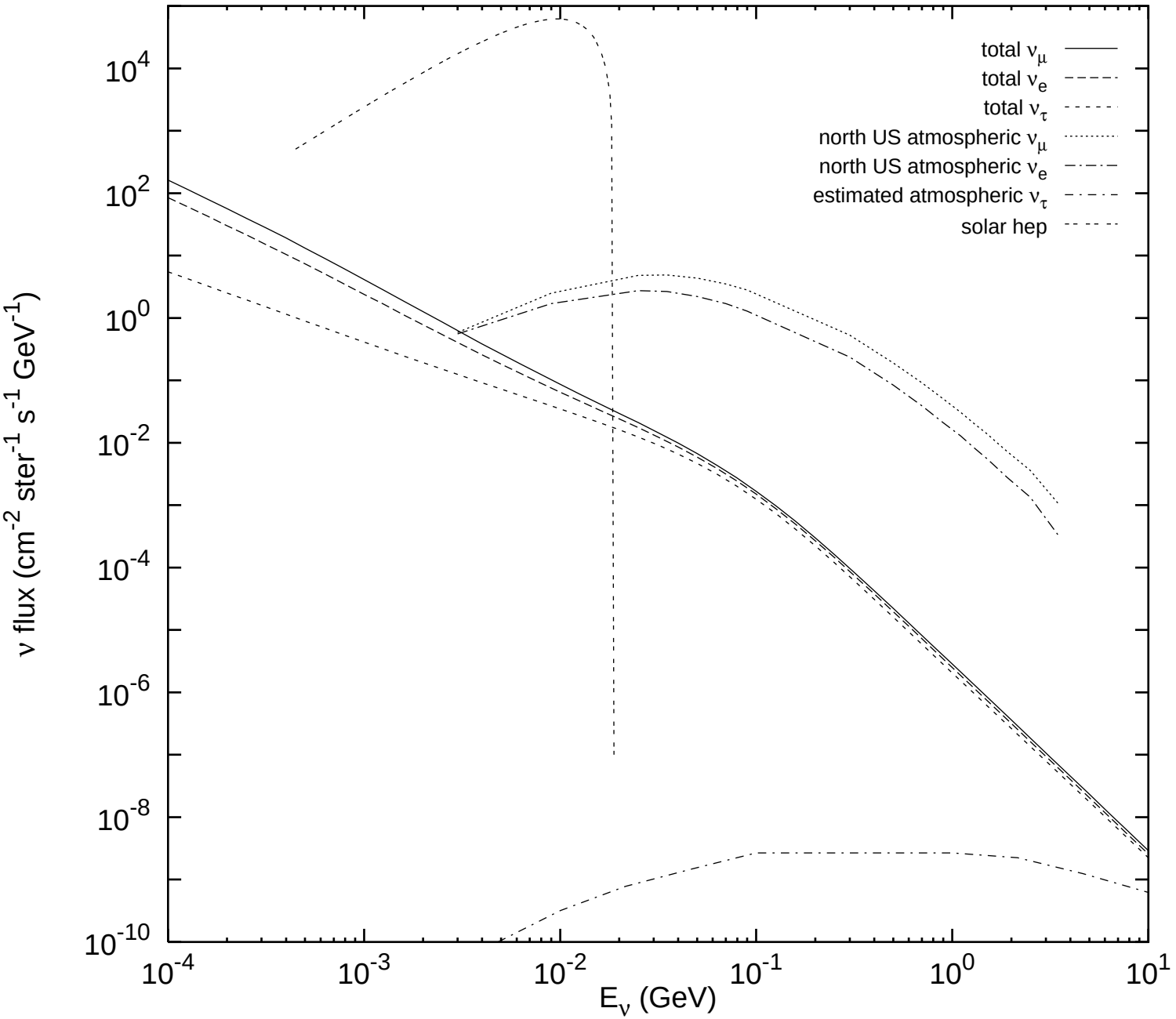
total ν_μ
total ν_e
total ν_τ
north US atmospheric ν_μ
north US atmospheric ν_e
estimated atmospheric ν_τ
solar hep
ν flux (cm^{-2} ster^{-1} s^{-1} GeV^{-1})
E_ν (GeV)
10^{4}
10^{2}
10^{0}
10^{-2}
10^{-4}
10^{-6}
10^{-8}
10^{-10}
10^{-4}
10^{-3}
10^{-2}
10^{-1}
10^{0}
10^{1}

This figure "fig1-3.png" is available in "png" format from:

http://arxiv.org/ps/hep-ph/9502268v1

Figure 4

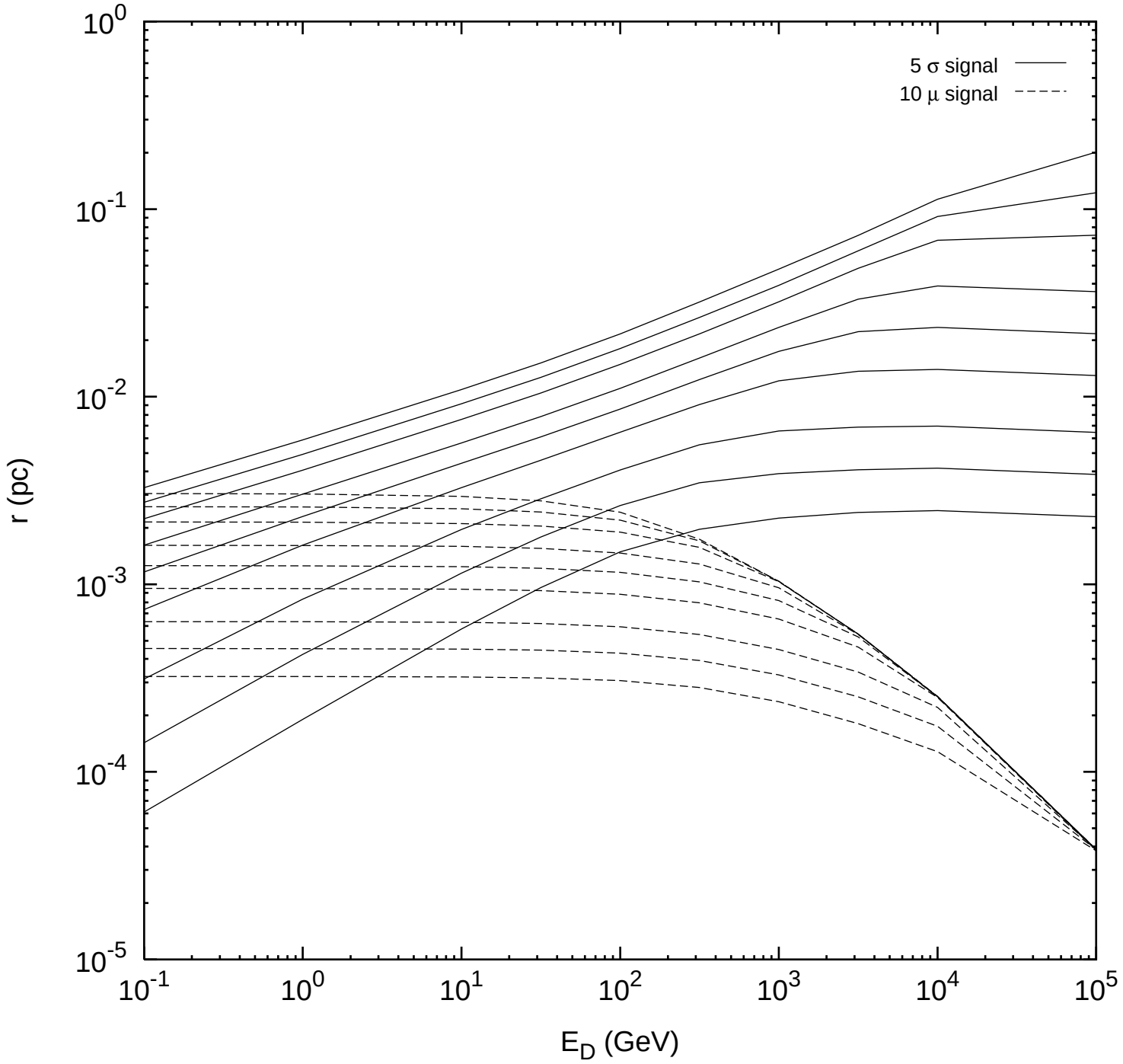
5 σ signal
10 μ signal
r (pc)
E_D (GeV)
10^0
10^-1
10^-2
10^-3
10^-4
10^-5
10^-1
10^0
10^1
10^2
10^3
10^4
10^5

This figure "fig1-4.png" is available in "png" format from:

http://arxiv.org/ps/hep-ph/9502268v1

Figure 5

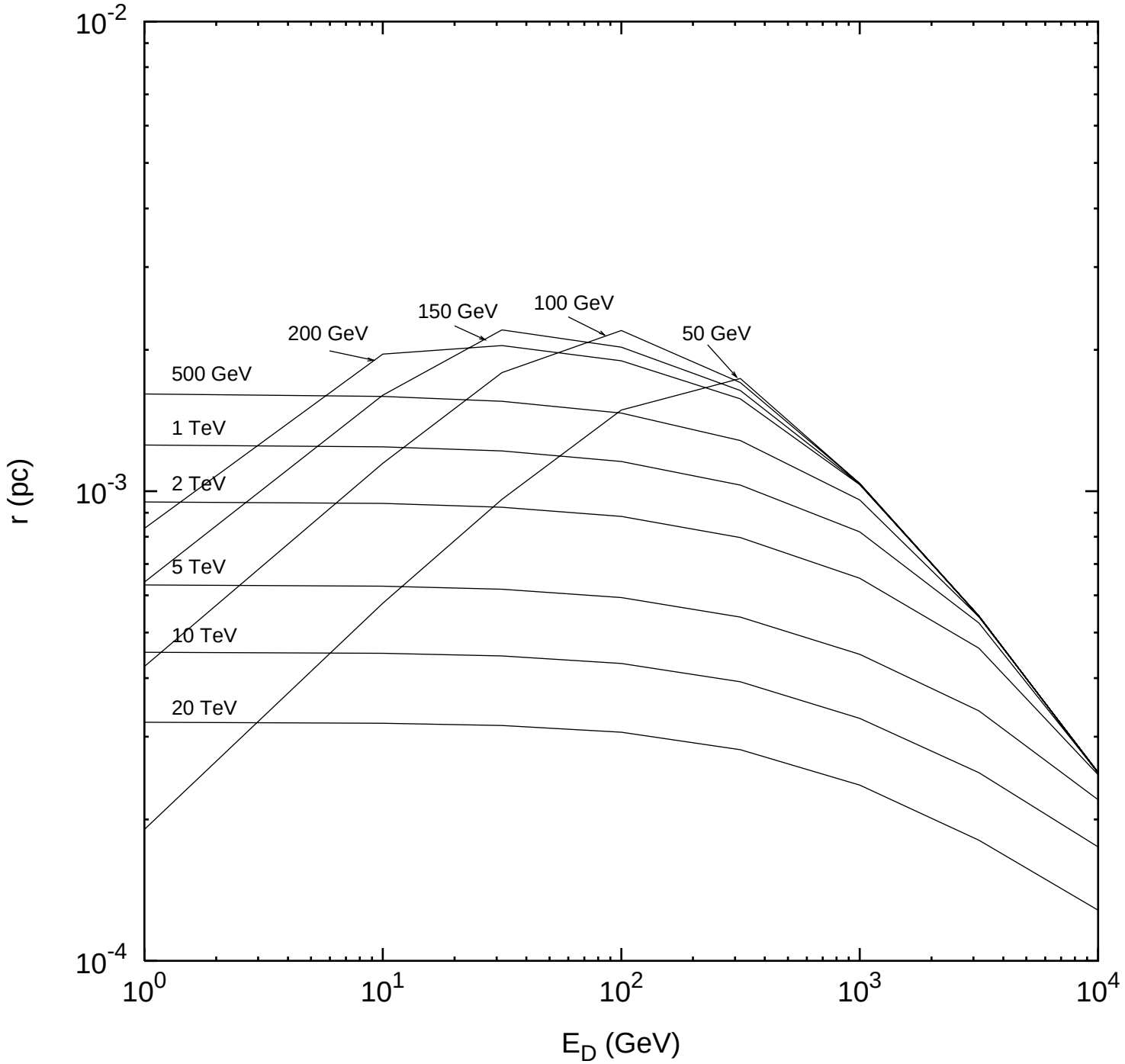
10^{-2}
10^{-3}
10^{-4}
r (pc)
10^0
10^1
10^2
10^3
10^4
E_D (GeV)
200 GeV
150 GeV
100 GeV
50 GeV
500 GeV
1 TeV
2 TeV
5 TeV
10 TeV
20 TeV

This figure "fig1-5.png" is available in "png" format from:

http://arxiv.org/ps/hep-ph/9502268v1

This figure "fig1-6.png" is available in "png" format from:

http://arxiv.org/ps/hep-ph/9502268v1

This figure "fig1-7.png" is available in "png" format from:

http://arxiv.org/ps/hep-ph/9502268v1

This figure "fig1-8.png" is available in "png" format from:

http://arxiv.org/ps/hep-ph/9502268v1

This figure "fig1-9.png" is available in "png" format from:

http://arxiv.org/ps/hep-ph/9502268v1